



Adsorption of methylene blue using sodium carboxymethyl cellulose-g-poly (acrylamide-co-methacrylic acid)/Cloisite 30B nanocomposite hydrogel

Hamzeh Khatooni¹ · Seyed Jamaledin Peighambaroust¹ · Rauf Foroutan¹ · Reza Mohammadi² · Bahman Ramavandi³

Accepted: 28 September 2022 / Published online: 29 October 2022

© The Author(s), under exclusive licence to Springer Science+Business Media, LLC, part of Springer Nature 2022

Abstract

A new adsorbent of CMC-g-Poly(MAA-co-AAm)/Cloisite 30B (Hyd/C30B) nanocomposite hydrogel was synthesized by the free radical polymerization approach to eliminate methylene blue (MB) dye from wastewater samples. The BET value for C30B, Hyd, and Hyd/C30B was determined 5.00, 0.83, and 2.42 m²/g, respectively, while, based on the MB removal method, the surface area for the mentioned adsorbents was calculated 133.12, 129.53, and 149.61 m²/g, respectively. The generated nano-hydrogel belonged to a type IV isotherm and had a pore size of 2–50 nm. In the MB adsorption process using the desired adsorbents, the maximum adsorption was attained at pH 8, temperature of 45 °C, time of 30 min, adsorbent dose of 0.8 g/L, and dye concentration of 10 mg/L. The swelling rate of the studied hydrogel depended on pH and temperature. The adsorption process increased with increasing temperature. The Gibbs free energy parameter and enthalpy had negative values, indicating that the degree of the spontaneity of the adsorption process increased at high temperatures. The data followed pseudo-second-order kinetic and Langmuir isotherm. The maximum MB adsorption using Hyd, Hyd/C30B, and C30B was computed to be 67.11 mg/g, 77.51 mg/g, and 70.42 mg/g, respectively. The adsorbents had a good ability to reduce industrial wastewater pollutants.

Keywords Hydrogel · Copolymer · Cloisite 30B · Adsorption

Introduction

Cationic dyes are toxic because they contain aromatic rings [1]. Methylene blue (MB) is a common cationic dye and used for the tinting of cotton, wool, and silk. Releasing this dye to the environment can interfere with the humans life and living organisms [2, 3]. Accordingly, it is necessary

to decrease MB from an aqueous media before discharge into the environment.

The physicochemical methods are more interesting among other methods due to their low cost, ease of operation, and high achievement [4]. Various materials have been proposed for the dye adsorption from aqueous solutions, of which hydrogels are one of the most commonly used adsorbents. Hydrogels are hydrophilic polymers with 3D networks that are bonded together by chemical or physical crosslinking and can sorb large amounts of water in their structure [5]. High swelling hydrogels causes capillary impact and osmotic pressure due to the presence of -NH₂, -COOH, -OH, -CONH₂, -CONH, and -SO₃H [5]. Hydrogels have applied in various fields like agriculture (controlled fertilizer release) [6], water storage, soil ventilation [7], water/ wastewater treatment [8], and medicine [9]. In the synthesis of hydrogels, the use of biopolymers such as sodium alginate, chitosan, Arabic gum, and xanthan gum has attracted consideration due to their availability, low cost, and biodegradability [10]. However, it should be noted that

✉ Seyed Jamaledin Peighambaroust
j.peighambaroust@tabrizu.ac.ir

✉ Bahman Ramavandi
b.ramavandi@bpums.ac.ir

¹ Faculty of Chemical and Petroleum Engineering, University of Tabriz, Tabriz 5166616471, Iran

² Polymer Research Laboratory, Department of Organic and Biochemistry, Faculty of Chemistry, University of Tabriz, Tabriz, Iran

³ Systems Environmental Health and Energy Research Center, The Persian Gulf Biomedical Sciences Research Institute, Bushehr University of Medical Sciences, Bushehr, Iran

synthesized hydrogels based on biopolymers, compared to synthetic polymers, have serious limitations like low hydrodynamic volume, poor thermal stability, lower surface area, and poor mechanical strength [10]. Therefore, the strength of polymer-based hydrogels should be improved. Copolymerization with synthetic polymers or modification with nanoparticles is a method for modifying biopolymers. One of the monomers used in the synthesis of copolymers and easily copolymerized with methacrylic acid monomer (MAA) is the acrylamide (AAm) monomer. The methacrylic acid monomer is composed of vinyl and carboxyl groups, which easily copolymerized with AAm monomer and can improve its properties [11].

In addition to copolymerization, the addition of minerals like clay to polymers can improve their mechanical performance, fire resistance, and thermal and electrical conductivity [12]. In recent years, clay minerals such as attapulgite [13], bentonite [14], kaolin [14], and montmorillonite (MMT) have been used to promote the physical and mechanical characteristics of hydrogels [15]. MMT has caused more attention in the preparation of hydrogels due to recyclability, free of biological contamination, low toxicity, and modification of polymer properties. Cloisite 30B (C30B) is a type of MMT. The MMT surface is modified with an organic surfactant called methyl tallow bis-(2-hydroxyethyl) of quaternary ammonium salt [16] and can be used as a suitable choice in modifying the properties of hydrogels.

According to the latest searches on reputable scientific sites, the adsorption performance of nanocomposite adsorbents prepared from CMC-g-Poly(MAA-co-AAm) and C30B, especially for MB dye removal, is still unclear. Therefore, in this investigation, the main aim was to synthesize CMC-g-Poly(MAA-co-AAm) hydrogel (Hyd) and CMC-g-Poly(MAA-co-AAm)/C30B nanocomposite hydrogel (Hyd/C30B) by graft copolymerization of MAA and AAm monomers along the CMC chain. The special goals were designed to (1) evaluate the effects of different ratios of AAm and MAA monomers to CMC and different C30B values on hydrogel structure (swelling factor) and MB adsorption from aqueous media; (2) assess the effect of various parameters on adsorption; (3) study the adsorption behavior using isotherm and kinetics models; and (4) explore the reusability and wastewater treatment capability of the nanocomposite hydrogel.

Experimental

Materials

Methacrylic acid monomer ($C_4H_6O_2$, analytical reagent, 98%, MW: 86.09 g/mol), acrylamide monomer ($CH_2CHCONH_2$, AAm, analytical reagent, 98%, MW:

71.08 g/mol) methylene blue ($C_{16}H_{18}ClN_3S$, MW: 319.86 g/mol, λ_{max} : 665 nm), sodium hydroxide (NaOH, analytical reagent, > 99%, MW: 39.99 g/mol), and hydrochloric acid (HCl, analytical reagent, 37%, MW: 36.45 g/mol) were purchased from Merck Co., Germany. Carboxymethyl cellulose biopolymer (CMC) and potassium persulfate ($K_2S_2O_8$, KPS, analytical reagent, $\geq 99\%$, MW: 270.32 g/mol) were prepared from Samchun (Korea). N–N-methylene bis-acrylamide (MBA, analytical reagent, 98%, MW: 154.17 g/mol) was purchased from Sigma-Aldrich (USA). The C30B nanoclay was purchased from Southern Clay Products Inc. (USA).

Synthesis of adsorbents

Hyd/C30B was synthesized using the free radical graft copolymerization method. For this purpose, an exact amount of C30B nanoclay was first added to 15 mL of deionized water and stirred for 3 h. At the end of this time, 1 g of CMC biopolymer was dissolved in 20 mL of deionized water and then C30B suspension was added (mixture A). After preparation of mixture A, a certain amount of MAA (with a neutralization degree of 75%) and AAm monomers were dissolved in 8 mL of deionized water (mixture B), and 0.03 g of MBA as a cross-linker was dissolved in 5 mL of deionized water and added into mixture B. Then, mixture B was added to mixture A and stirred for 30 min under a nitrogen atmosphere for deoxygenation and placed in a thermostatic bath at 70 °C. After, 0.1 g of KPS was then added to the general mixture (mixture A + mixture B) as an initiator under a nitrogen atmosphere and placed at 70 °C for 3 h to complete the free radical polymerization reaction. At the end of this time, the nanocomposite hydrogel produced was washed with ethanol and deionized water and placed at 55 °C for a day to dry completely. After drying, the nanocomposite hydrogel was pulverized using a mill and granulated using sieve No. 25 (ASTM E11), and stored in anti-humidity polyethylene containers at room temperature. Synthesis of hydrogel without nanoclay has been done according to the mentioned method, with the difference that C30B nanoclay has not been used in its preparation. Figure 1 shows the mechanism for the synthesis of the desired nanocomposite hydrogel.

Swelling determination

To check the swelling rate of the desired hydrogel sample, 1 g/L of the desired hydrogel sample was immersed in 100 mL of deionized water for 24 h at a temperature of 25 °C. After 24 h, the swollen hydrogels were removed from the deionized water and weighed using a digital scale. The equilibrium water absorption capacity (W_{eq} , g/g) was determined using the following equation [17]:

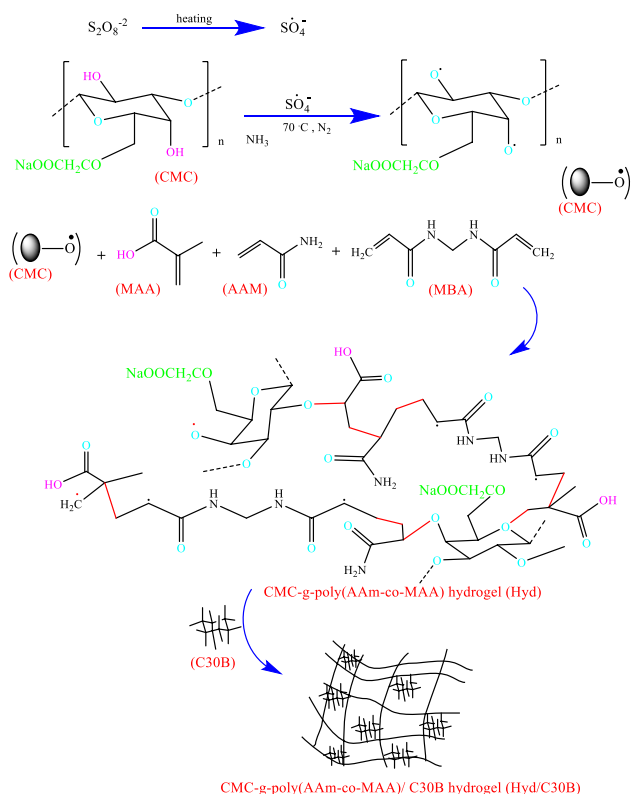


Fig. 1 Proposed reaction mechanism for the synthesis of Hyd and Hyd/C30B

$$W_{eq} = \frac{W_s - W_i}{W} \quad (1)$$

where W_i and W_s are the weight of the dry and swollen hydrogel samples, respectively.

MB adsorption tests

The adsorption of MB cationic dye was done in the batch system using C30B, Hyd, and Hyd/C30B, and the effect of the weight ratio of MAA/AAm monomers and the amount of CMC to the total MAA/AAm monomers on the MB adsorption was studied. After determining the optimal value of CMC and the weight ratio of MAA to AAm monomers, the effect of effective parameters (pH, temperature, contact time, adsorbent dose, and dye concentration) on the adsorption percentage was investigated. To evaluate the impact of pH, the adsorption study was performed in pH 2–10 and in conditions such as MB concentration of 10 mg/L, adsorbent dose of 0.8 g/L, contact time of 30 min, temperature of $25\text{ }^\circ\text{C}$, and mixing speed of 300 rpm. After that, the effect of other parameters like temperature ($25\text{--}45\text{ }^\circ\text{C}$), time (10–120 min), adsorbent dose (0.4–1.22 g/L), and dye content (10–50 mg/L) was also examined at the optimum pH value. At each step after the adsorption process, the

residual dye in an aqueous solution was measured using a UV–vis spectrophotometer and at a maximum wavelength of 665 nm. The adsorption process was performed with three iterations and the average of the data was presented as the desired result. The MB adsorption (%) and equilibrium adsorption capacity (q_e , mg/g) of the adsorbents were determined by the following formulas:

$$\text{MB adsorption(\%)} = \frac{[MB]_{\text{initial}} - [MB]_{\text{final}}}{[MB]_{\text{initial}}} \quad (2)$$

$$q_e = \frac{([MB]_{\text{initial}} - [MB]_{\text{final}}) \cdot \text{Volume}}{\text{Adsorbent weight}} \quad (3)$$

Results and discussion

Adsorbents property

The FTIR spectra for CMC, C30B, Hyd, and Hyd/C30B before and after the MB adsorption are shown in Fig. 2a,b. An absorption peak in the wavelengths of $3846\text{--}3439\text{ cm}^{-1}$ has been observed in the structure of CMC, Hyd, and Hyd/C30B, which is related to the tensile vibrations of the -OH and N–H groups [18]. Also, the absorption peak at 2908 and 1328 cm^{-1} appearing in the CMC structure is attributed to the tensile and flexural vibrations of the -CH group and the peak appearing at 1059 cm^{-1} is linked to C–O–C [19]. The peaks at $1546\text{--}1612\text{ cm}^{-1}$ and $1465\text{--}1422\text{ cm}^{-1}$ related to -COO and carboxylate anions [20]. After the formation of hydrogel, a new absorption peak at 1695 cm^{-1} was observed, which is attributed to the -C=O group and confirms the successful bonding of MAA and AAm with the CMC structure. In addition, the absorption peak at 1166 cm^{-1} shows the C–N tensile vibration in the MBA structure [17], accordingly, it can be stated that the desired hydrogel has been successfully synthesized. The absorption peak observed at $1651\text{--}1662\text{ cm}^{-1}$ belongs to carboxamide group in AAm [21], which confirms the production of hydrogel. In the structure of synthesized hydrogels, the vibration peaks appearing at 954 and 764 cm^{-1} are related to -C–O–C- and carboxyl groups in the acrylate structure, respectively [22]. Peaks have appeared in 1642 and 3396 cm^{-1} are related to -OH tensile vibrations in C30B and Hyd/C30B [23]. In addition, peaks of 1044 and 524 cm^{-1} have appeared in the C30B structure, which represent the tensile vibrations of Si–O and Al–O, respectively [23]. After the formation of the Hyd/C30B nanocomposite hydrogel, peaks appeared at 525 and 1060 cm^{-1} are attributed to the presence of C30B nanoclay in the desired nanocomposite hydrogel. A shift in the position and intensity of peaks in Hyd/C30B can be due to interactions between

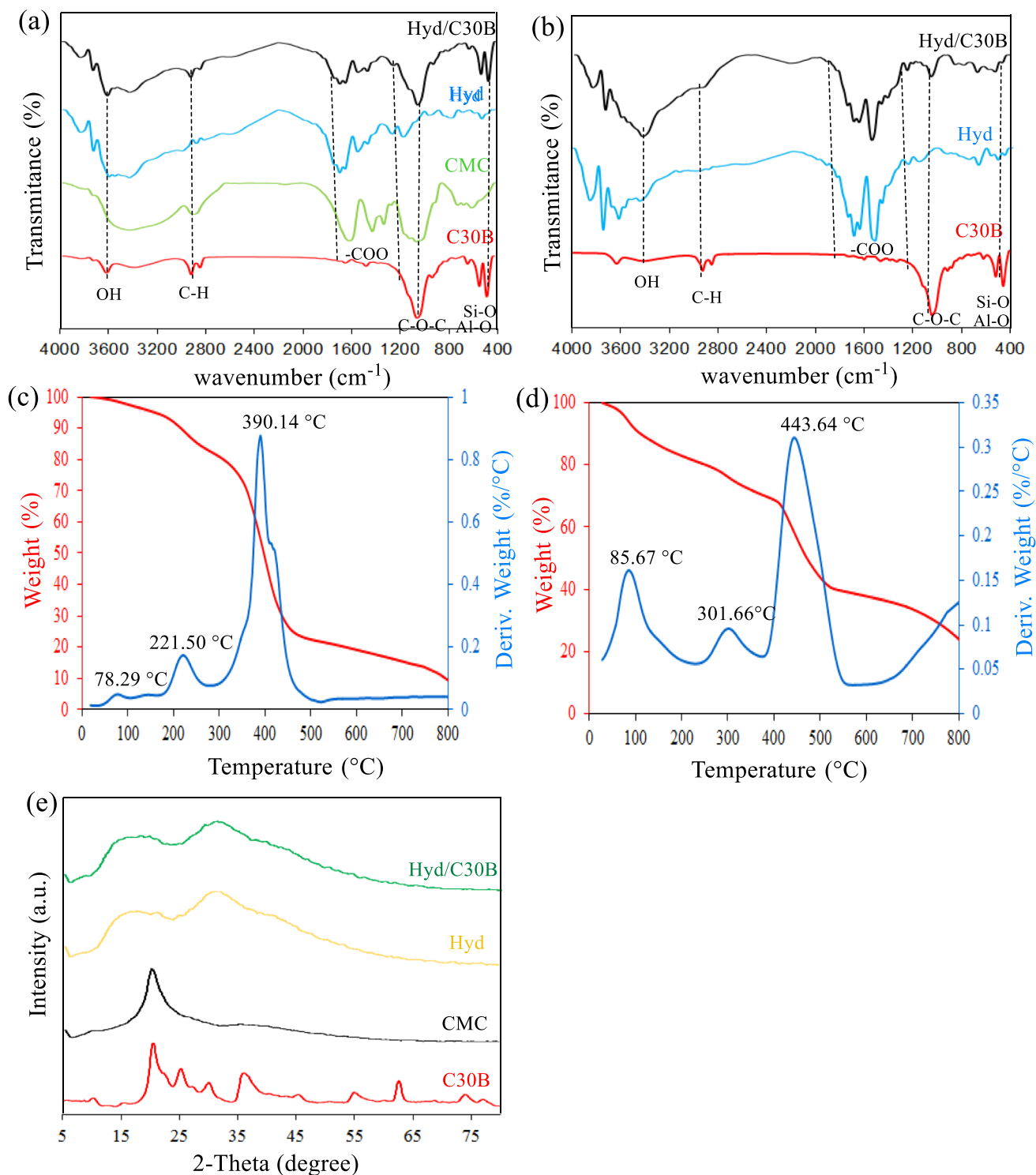


Fig. 2 (a) FTIR for fresh C30B, CMC, Hyd, and Hyd/C30B, (b) FTIR for used C30B, CMC, Hyd, and Hyd/C30B, (c) TGA-DTG for Hyd (d) TGA-DTG for Hyd/C30B, and (e) XRD for C30B, CMC, Hyd, and Hyd/C30B

the functional groups of the components of the hydrogels (C30B and Hyd). After the adsorption process, the changes in the functional groups in the structure of C30B, Hyd, and Hyd/C30B samples were negligible, indicating that the

interaction between the MB molecule and the structure of the samples was due to weak van der Waals bonds and π - π , which indicates the existence of physical interactions [24].

The thermal stability (TGA analysis) results for Hyd and Hyd/C30B samples are shown in Fig. 2c,d. Based on the desired figure, the samples in the temperature of 45–800 °C have three steps of weight loss. The initial step of weight loss for Hyd and Hyd/C30B samples was performed at 45–205 °C and 45–245 °C, respectively, which is related to water evaporation and breaking of C–O–C bonds in the CMC structure forming the target hydrogels [25]. The second weight loss has occurred at 205–345 °C and 240–410 °C for Hyd and Hyd/C30B samples, respectively, which is due to the destruction of the side chain and the CO₂ adsorption from the main polymer chain [26]. Based on the TGA results, the highest amount of weight loss occurred in the second stage and the Hyd/C30B nanocomposite sample had less weight loss compared to Hyd, which could be due to the presence of C30B clay nanoparticles in the hydrogel.

Based on the XRD (Fig. 2e), a high-intensity peak is seen in the CMC structure at 2θ : 20.35°, which confirms the presence of the crystal in the CMC structure [27]. It is noticeable that the crystals in CMC are due to intramolecular hydrogen bonds between the hydroxyl and carboxylic functional groups. Also, the XRD diffraction pattern in the synthesized Hyd structure shows two peaks at 2θ = 21.6 and 30.7°, which could be due to CMC in the desired hydrogel structure and the bonding of vinyl monomers with CMC, which can reduce intramolecular hydrogen bonds and crystals in CMC [21]. For C30B sample, peaks have been observed at 2θ : 5–80°, which corresponded to the silicate layers in the C30B nanoclay structure. According to the results, after the formation of Hyd/C30B, the peaks related to C30B have disappeared, which indicates the exfoliated and uniform dispersion of C30B nanoclay layers among the polymer chains forming the hydrogel [17].

SEM and EDX-Map test are drawn in Fig. S1. The results showed that C30B nanoclay has a layered structure with different pores and unevenness and also contains elements of Si, C, O, and Al (Fig. S1a-c). As the results show, the synthesized Hyd has an almost smooth surface and most of its structure consists of C and O (Fig. S1d-f). After the formation of Hyd/C30B nanocomposite, sheets are formed on the surface of the desired hydrogel that does not exist on the Hyd surface, which can indicate the presence of C30B silicate plates in the nanocomposite structure (Fig. S1g). To confirm the presence of C30B nanoclay in the Hyd/C30B nanocomposite, EDX-Map analyzes were also applied, which confirmed the presence of Si and Al elements in the Hyd/C30B hydrogel (Fig. S1h-i). After the MB adsorption using Hyd, Hyd/C30B, and C30B, the pores and unevenness in the surface of the samples were reduced (Fig. S1k-m). Changes in the samples can be linked to the placement of MB on the adsorbents, which confirms the ability of the samples to absorb MB from the water.

To determine the surface properties of C30B, Hyd, and Hyd/C30B, the N₂ adsorption–desorption isotherm was utilized and the results are provided in Fig. 3. Based on the results, the BET value for C30B, Hyd, and Hyd/C30B samples was 5.009, 0.831, and 2.422 m²/g, respectively. The Hyd/C30B nanocomposite has a high activity level compared to Hyd, which can be due to the presence of C30B nanoclay in the structure of the desired hydrogel network. In addition, the N₂ adsorption–desorption isotherm for the samples has a residual loop of type H3, which according to the IUPAC classification, the materials are belonged to type IV isotherm [28]. Also, the pore size for the mentioned samples was determined in the range of 2–50 nm, and according to the IUPAC report, the mentioned materials are classified as mesoporous materials. Although the N₂ adsorption–desorption isotherm is a common method for measuring the specific surface of samples, this method is not efficient for determining the specific surface of hydrogel samples, because the structure and pores of hydrogels change due to drying. In addition, hydrogels have elastic properties and when placed in aqueous solutions, they swell and their active surface area increases compared to their dried state. Thus, according to the mentioned evidence and reasons, it can be proposed that the N₂ adsorption–desorption method is not efficient for determining the specific level of hydrogel samples. One of the other methods used in previous studies to determine the size of the specific area is based on the methylene blue dye removal (S_{MB}). In this method, the specific surface area is determined using Eq. (4) [29]:

$$S_{MB} = S_{MB}^0 \times q_{max} \quad (4)$$

Here, S_{MB}⁰ the surface needed for removal of methylene blue dye molecule (1.93 m²/mg) and q_{max} is the maximum capacity of the MB removal (mg/g). Based on the mentioned method, the specific surface area for C30B, Hyd, and Hyd/C30B samples was determined to be 133.12, 129.53, and 149.61 m²/g, respectively.

Effect of weight ratio of monomers

The hydrogel properties like swelling and ability to adsorb pollutants can be affected by the amount of natural polymer, inorganic part, and monomers in the studied hydrogel. The amount of swelling in polymeric hydrogel systems depends on various factors like pores, functional groups, and the intermolecular space in the hydrogel [30]. In the current study, the optimal parameters were determined and reported based on swelling value and MB adsorption efficiency. Figure 4a shows the effect of increasing the weight ratio of total monomers, MAA/AAM to CMC in the range of 4–8 g/g CMC. By increasing the weight ratio of the total monomers

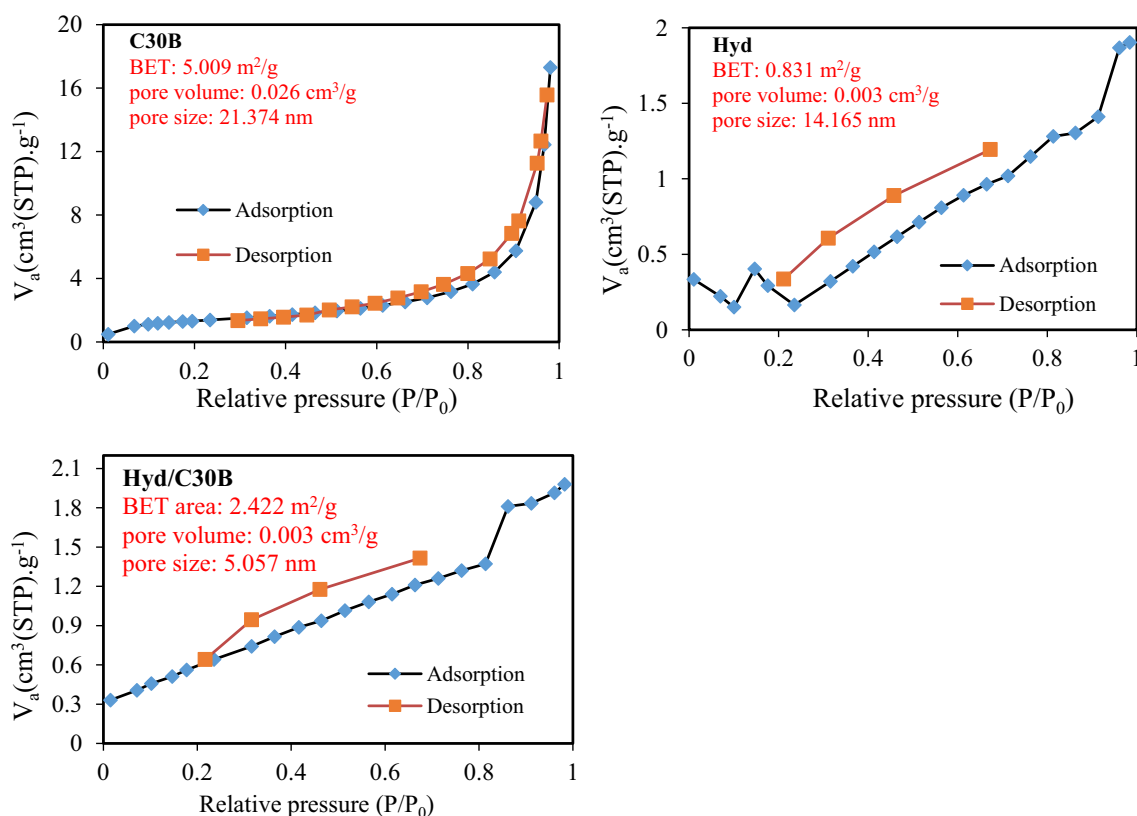


Fig. 3 N₂ adsorption–desorption isotherm for C30B, Hyd, and Hyd/C30B samples

to CMC to a weight ratio of 6 (Monomers: CMC → 6:1), the swelling value and the MB adsorption increased, which can increase the aggregation of two monomer molecules around the CMC chain noted that it increases the bonding of monomer molecules (MAA/AAm) on the main CMC chain and increases the hydrophilicity of the hydrogel network [13]. In addition, it should be noted that with increasing the weight ratio of total MAA/AAm monomers to CMC by more than 6, the amount of swelling and adsorption efficiency has decreased. Although the hydrophilicity of the hydrogel system should increase with increasing the total amount of MAA/AAm monomers, the results showed that the amount of swelling and the maximum adsorption efficiency decreased. The decrease in the adsorption efficiency and swelling value of the synthesized hydrogel network can be due to increasing the tendency to form homopolymers of monomers instead of forming the graft copolymer structure and increasing the transfer of polymer chains to monomer molecules, which has been expressed in previous studies [31].

Another structural factor that can affect the amount of swelling value and the adsorption efficiency is the ratio of monomers. In Fig. 4b, the effect of the weight ratio of MAA to AAm monomers in different ratios on the adsorption efficiency and the value of hydrogel swelling

was investigated. The results showed that by increasing the amount of MAA to AAm the swelling value and the adsorption rate increased. This increasing rate could be justified by the increase of $-\text{COO}^-$ groups compared to $-\text{CONH}_2$ groups, which improves the hydrophilicity of the hydrogel network and increases the dehydration of hydrogels [32]. The presence of $-\text{COO}^-$ groups with increasing the amount of MAA can also increase the efficiency of the adsorption process, because electrostatic force arises between MB and $-\text{COO}^-$.

Figure 4c shows the effect of different weight percentages of C30B nanoclay (1.5–10%) on the amount of swelling and adsorption rate. As the results show, adding 1.5 wt.% of C30B nanoclay to the hydrogel network increases the swelling value and the adsorption percentage, which can be corresponded to the electrostatic repulsion force between the anionic groups of C30B and the negative groups of the chains [33]. However, it should be noted that increasing the amount of C30B in the hydrogel network from 1.5 to 10 wt.% has reduced the value of swelling and MB adsorption using the desired polymer system. A decrease in swelling rate and adsorption performance of the nanocomposite hydrogel can be due to increased crosslinking of polymer chains with C30B nanoclay, which results in higher compaction of hydrogel structure [34]. Therefore, 1.5 wt.% of C30B

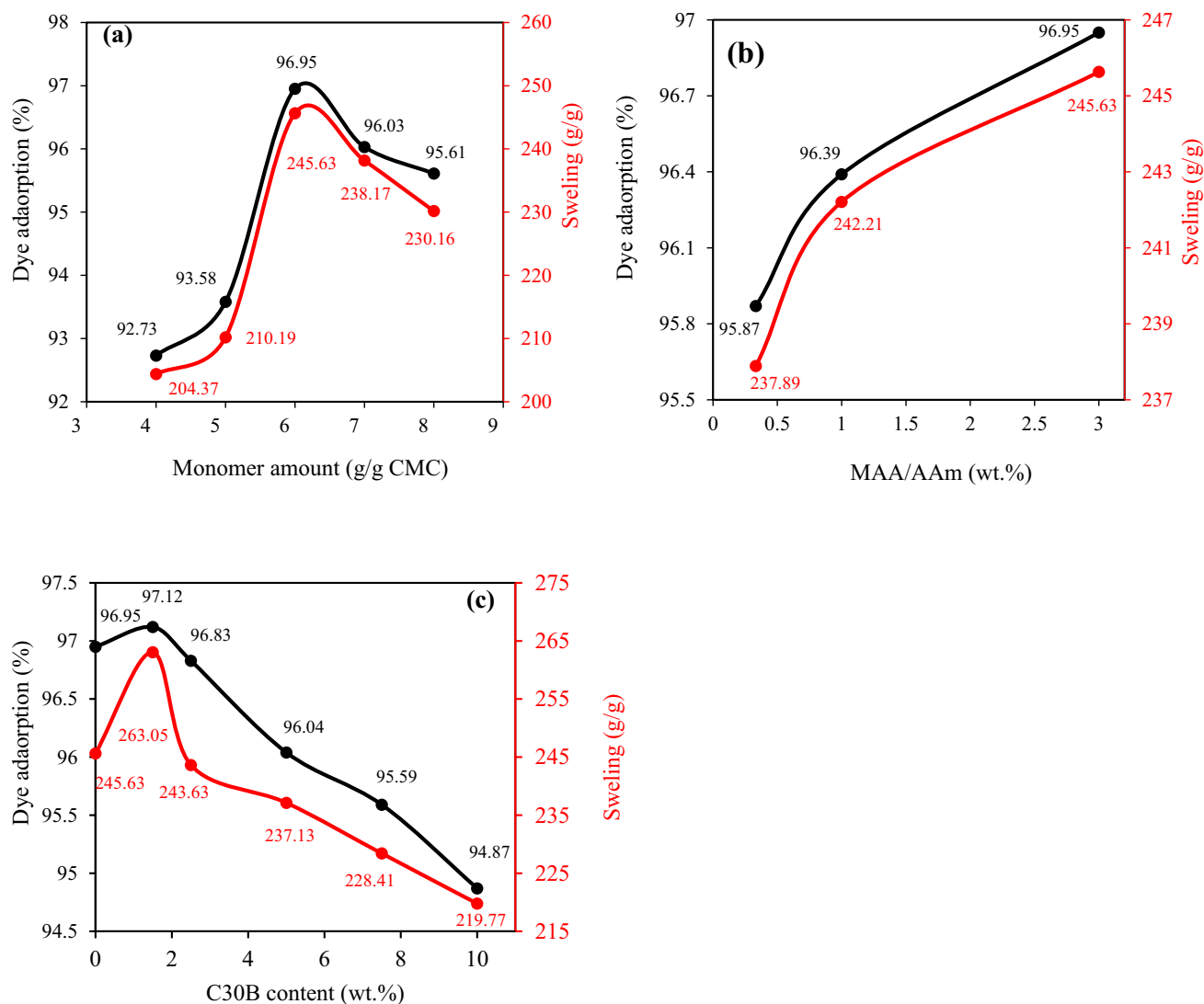


Fig. 4 (a) Effect of weight ratio of CMC to total MAA/AAm, (b) weight ratio of MAA to AAm, (c) weight ratio of C30B nanoclay in the polymer matrix (swelling test conditions; temperature: 25 °C,

pH: 6.6, time: 180 min, and adsorption test conditions; temperature: 25 °C, pH: 6, MB concentration: 10 mg/L, adsorbent dose: 0.8 g/L, time: 30 min, mixing speed: 500 rpm)

nanoclay was selected as the optimal value for production of the nanocomposite hydrogel.

Effect of adsorbent quantity and pH

The dose of adsorbents is an effective parameter for removing dye from water, which determines the amount of dye eliminated by the adsorbent and the cost of the process [35]. Also, the availability of active sites on the adsorbent surface is the main stimulus for dye adsorption from an aqueous solution [36]. In Fig. 5a, by elevating the adsorbent dose, the MB removal has increased. Increasing the dose of adsorbent increases the sites and area for MB to be located, which in turn increases the MB removal from water. It should also be noted that by increasing the adsorbent dose by more than

0.8 g/L, the removal process was almost proven due to the decrease of MB content in the aqueous phase, non-collision of MB molecules with active sites, and the collision and adhesion of the adsorbent particles with each other (reduce available surface) [37]. Therefore, according to the good efficiency obtained in the removal of MB by C30B nanoclay (99.17%), Hyd (98.57%), and Hyd/C30B (99.67%) at the adsorbent dose of 0.8 g/L, this dose was chosen as optimal.

The zero-charge point (pH_{zpc}) was obtained using zeta potential analysis and the results are presented in Fig. 5b. The pH_{zpc} value for Hyd, Hyd/C30B, and C30B was determined to be 5.8, 6.2, and 6.4, respectively. The samples had a positive and negative charge at pHs below and above pH_{zpc} , respectively. As depicted in Fig. 5c, at $\text{pH} < 6$, the adsorption efficiency is low and with increasing pH to 8, the

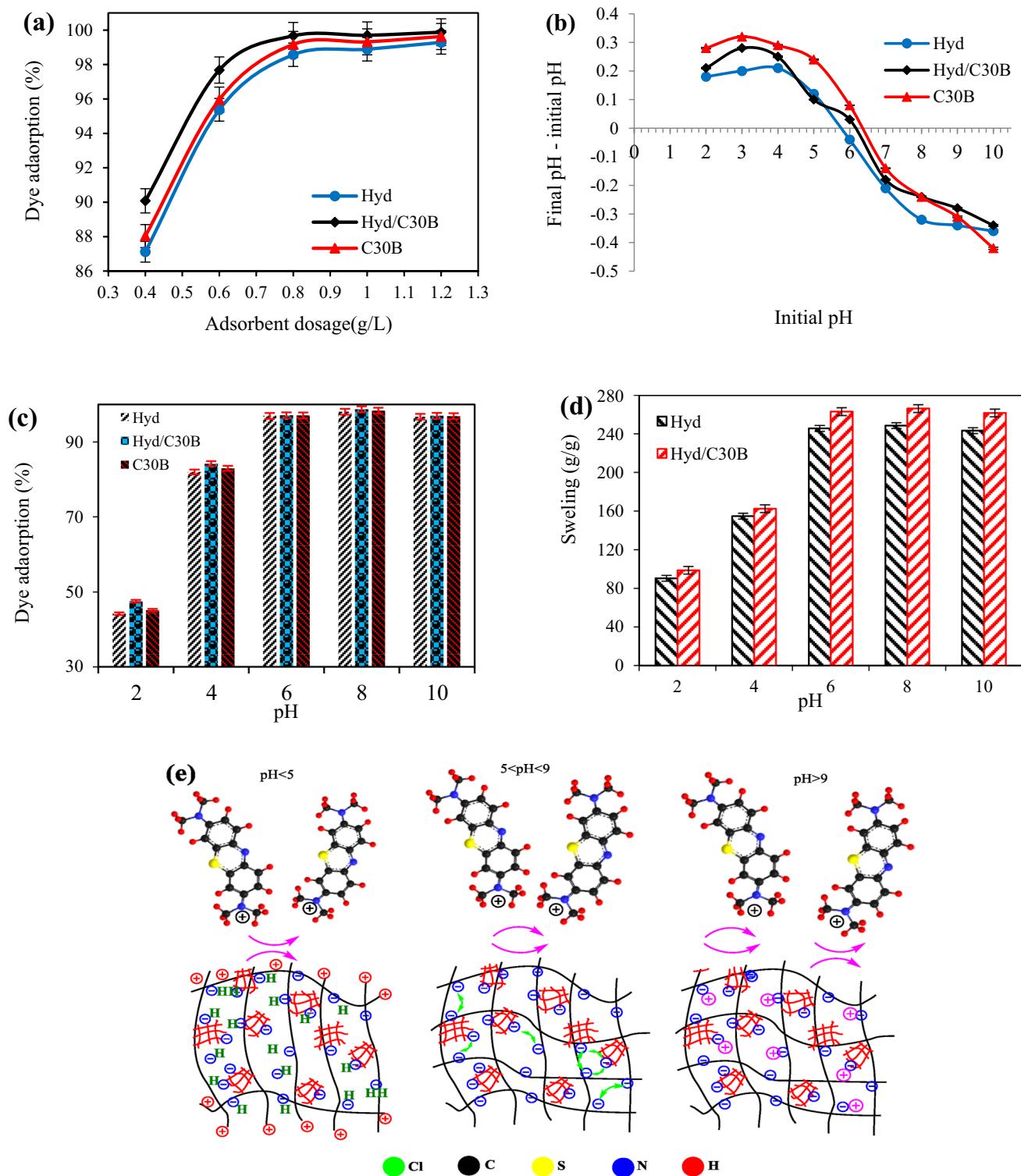


Fig. 5 (a) Effect of adsorbent dose, (b) different states of surface loads in the pH range of 2–10, (c,d) effect of pH on the removal efficiency and the swelling value of hydrogel, (e) MB adsorption mechanism using hydrogel in different pHs

adsorption efficiency is elevated. By increasing pH to 10, the MB adsorption using all three adsorbents was decreased. Decreased efficiency at acidic pH can be due to the high

concentration of H^+ and the protonation of active sites of adsorbents by these ions [38]. In addition to the presence of H^+ , another factor that can reduce the efficiency of hydrogel

systems at acidic pH is the amount of swelling, the results showed that at acidic pH, the value of hydrogel swelling is less due to the presence of H^+ ions (Fig. 5d). At basic pH of 8, the concentration of OH^- ions increases, and the amount of H^+ in water decreases, resulting in the release of sites occupied by H^+ ions, which makes more active sites in available for MB molecules [39]. In addition, by decreasing the amount of H^+ , the amount of swelling of the hydrogel systems increases, which can increase the available sites and area for the dye to be located, thus increasing the dye adsorption efficiency of MB by hydrogel adsorbents. Also, at high basic pH ($pH > 8$), although the surface charge of the adsorbents is negative and suitable for the adsorption of cationic dyes, the presence of large amounts of Na^+ in the dye solution leads to a slight decrease in the adsorption efficiency, because it causes to decrease the swelling of hydrogel systems. Figure 5e summarize the mechanism of the MB adsorption using hydrogel systems at different pHs.

Effect of temperature on efficiency, swelling, and thermodynamic study

Fig. S2a,b shows the impact of temperature on the swelling value of the desired hydrogel systems and the MB adsorption using the adsorbents in the temperature range of 25–45 °C. With increasing the temperature from 25 to 45 °C, the swelling ratio for Hyd and Hyd/C30B hydrogel systems increased from 248.53 and 266.21 g/g to 264.43 and 284.73 g/g, respectively, which can affect the adsorption efficiency. Increasing the temperature in the temperature range of 25–45 °C has also increased the efficiency of the MB adsorption. Increasing the efficiency of the adsorption process with increasing temperature can be due to the loosening of hydrogel networks [40], increasing the mobility of the dye molecules, and increasing the rate of dye penetration into the adsorbent structure [41]. Based on the results, the ability to remove MB using Hyd/C30B was higher than Hyd. Because the Hyd/C30B nanocomposite had higher swelling rate, more functional groups, and more active surface than the hydrogel. Fig. S2c shows the adsorption and swelling ability of Hyd and Hyd/C30B at 45 °C, which well shows the swelling and MB adsorption using Hyd/C30. Therefore, at 45 °C, as the optimal temperature, the maximum MB adsorption using C30B, Hyd, and Hyd/C30B was determined 99.17, 98.57, and 99.67%, respectively. The thermodynamic interpretation and results are provided in Table 1 and Supplementary information (including Fig. S2).

Effect of contact time and kinetics study

Figure 6a shows the effect of treatment time on the MB adsorption using Hyd, Hyd/C30B, and C30B. The adsorption process was performed in two stages (10–30 min and

Table 1 Thermodynamic parameters for the MB adsorption using the desired adsorbents

Adsorbent	T (°C)	ΔG° (kJ/mol)	ΔH° (kJ/mol)	ΔS° (kJ/mol.K)
Hyd	25	-10.265	11.713	0.074
	30	-10.633		
	35	-11.002		
	40	-11.370		
	45	-11.739		
Hyd/C30B	25	-11.331	57.315	0.230
	30	-12.482		
	35	-13.633		
	40	-14.785		
	45	-15.936		
C30B	25	-10.584	28.474	0.131
	30	-11.239		
	35	-11.894		
	40	-12.549		
	45	-13.204		

30–120 min). The first step was performed in the time range of 10–30 min, when the dye adsorption using Hyd, C30B, and Hyd/C30B increased from 86.94, 92.81, and 88.19 to 98.57, 99.67, and 99.17%, respectively, which has a relatively faster than the second one (30–120 min). This behavior can be explained by the saturation of active sites in the adsorbents with dye over time [42], the reduction of accessible active sites of adsorbents, and creation an electrostatic repulsion force between MB on the adsorbent surfaces and solution [43]. Therefore, 30 min was determined as the optimal time.

Kinetic study provides valuable information on the pathways and mechanisms of adsorption reactions [44]. During the MB removal using desired adsorbents, kinetic models of pseudo-first order (Eq. 5), pseudo-second order (Eq. 6), and intra-particle diffusion (Eq. 7) were studied:

$$\text{Pseudo - first - order : } \ln (q_e - q_t) = \ln q_e - k_1 \times t \quad (5)$$

$$\text{Pseudo - second - order : } \frac{t}{q_t} = \frac{1}{k_2 q_e^2} + \frac{1}{q_e} t \quad (6)$$

$$\text{Intra - particle diffusion : } q_t = k_{int} \cdot t^{0.5} + I \quad (7)$$

where, q_e (mg/g) and q_t (mg/g) are the MB adsorption capacity at equilibrium and time of t , respectively, k_1 is adsorption constant of pseudo-first order model (1/min), k_2 is the equilibrium constant velocity of the pseudo-second order model (g/mg.g), k_{int} is the intra-particle penetration rate constant (mg/g.min^{0.5}), and 'I' is the intercept of the linear curve (mg/g).

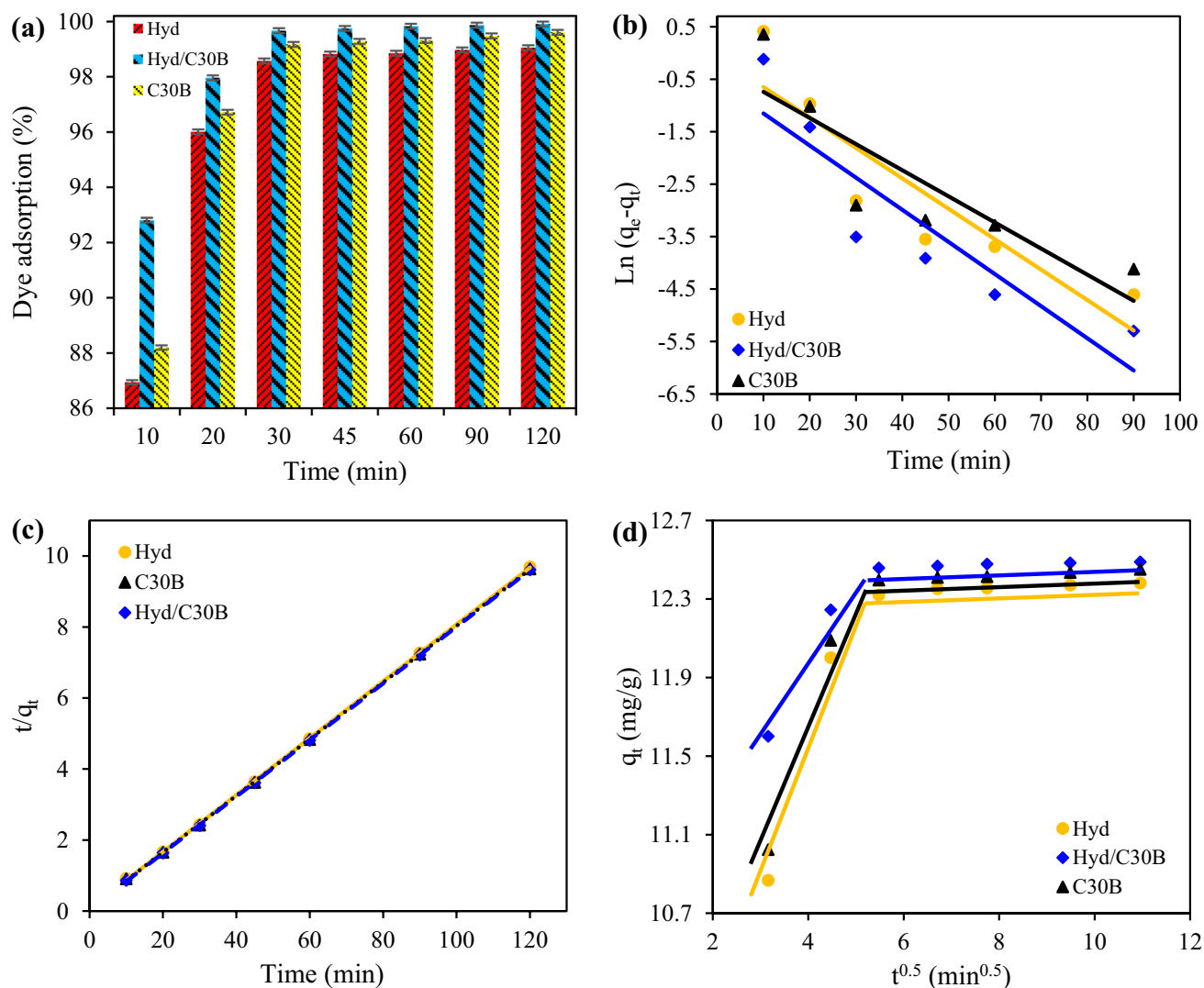


Fig. 6 (a) Effect of treatment time (pH: 8, temperature: 45 °C, adsorbent dose: 0.8 g/L, dye concentration: 10 mg/L, and mixing rate: 400 rpm) and kinetics models (b) pseudo-first order, (c) pseudo-second

order, and (d) intra-particle diffusion of MB removal using C30B, Hyd, and Hyd/C30B

Linear regression of pseudo-first order, pseudo-second order, and intra-particle diffusion models of MB adsorption using Hyd, Hyd/C30B, and C30B is shown in Fig. 6b-d. The kinetic constants and variables are reported in Table S1. The results showed that the R^2 value for the pseudo-second order model is higher than the pseudo-first order one. Also, $q_{e,cal}$ values of the pseudo-second order model are more consistent with $q_{e,exp}$ values. So, the kinetic behavior of the MB adsorption using desired adsorbents followed the pseudo-second order model. According to the pseudo-second order model, the velocity limiting step is considered chemical adsorption, including adsorption through the sharing or exchange of electrons between the adsorbent and the adsorbed [45]. Also, from the results reported in Table S1, it was observed that the values of $q_{e,cal}$ and $q_{e,exp}$ are not equal. Thus, the

diffusion stage within the particle may be involved in the mechanism of the adsorption process [46]. The results showed that the value of parameter 'I' for the MB adsorption using Hyd, Hyd/C30B, and C30B was not zero. This indicates that the velocity limiting phase is controlled by several adsorption mechanisms. The first stage occurs with a high slope, which involves the surface diffusion of dye molecules from the solution on the adsorbent surface, and the second stage, which has a lower slope, involves the diffusion of dye molecules into the adsorbent pores [46].

MB Concentration effect and equilibrium study

The effect of the MB content on the adsorption efficiency was studied using Hyd, Hyd/C30B, and C30B and the

results are reported in Fig. 7a. The MB adsorption efficiency decreased with increasing dye concentration. This trend can be due to the saturation of active sites on the adsorbent surface and the creation of electrostatic repulsion force between the adsorbent and soluble dye molecules [47].

The adsorption isotherm models describe how contaminants interact with adsorbents, so it is important to explain the adsorption mechanism, express the adsorption capacity, and design the adsorption systems [48]. Langmuir, Freundlich, and Temkin isotherm models were used to describe data (Eq. 8–10) [49]:

$$\text{Langmuir Model: } \frac{C_e}{q_e} = \frac{C_e}{q_m} + \frac{1}{q_m K_L}, R_L = \frac{1}{1 + K_L C_i} \quad (8)$$

$$\text{Freundlich: } q_e = K_f \cdot C_e^{\frac{1}{n}} \quad (9)$$

$$\text{Temkin Model: } q_e = B \ln K_T + B \ln C_e, B = \frac{R \times T}{b} \quad (10)$$

where, C_e implies equilibrium content of MB in solution (mg/L), q_m denotes maximum Langmuir adsorption capacity (mg/g), K_L is Langmuir adsorption constant, R_L implies separating coefficient, K_f implies Freundlich constant, n

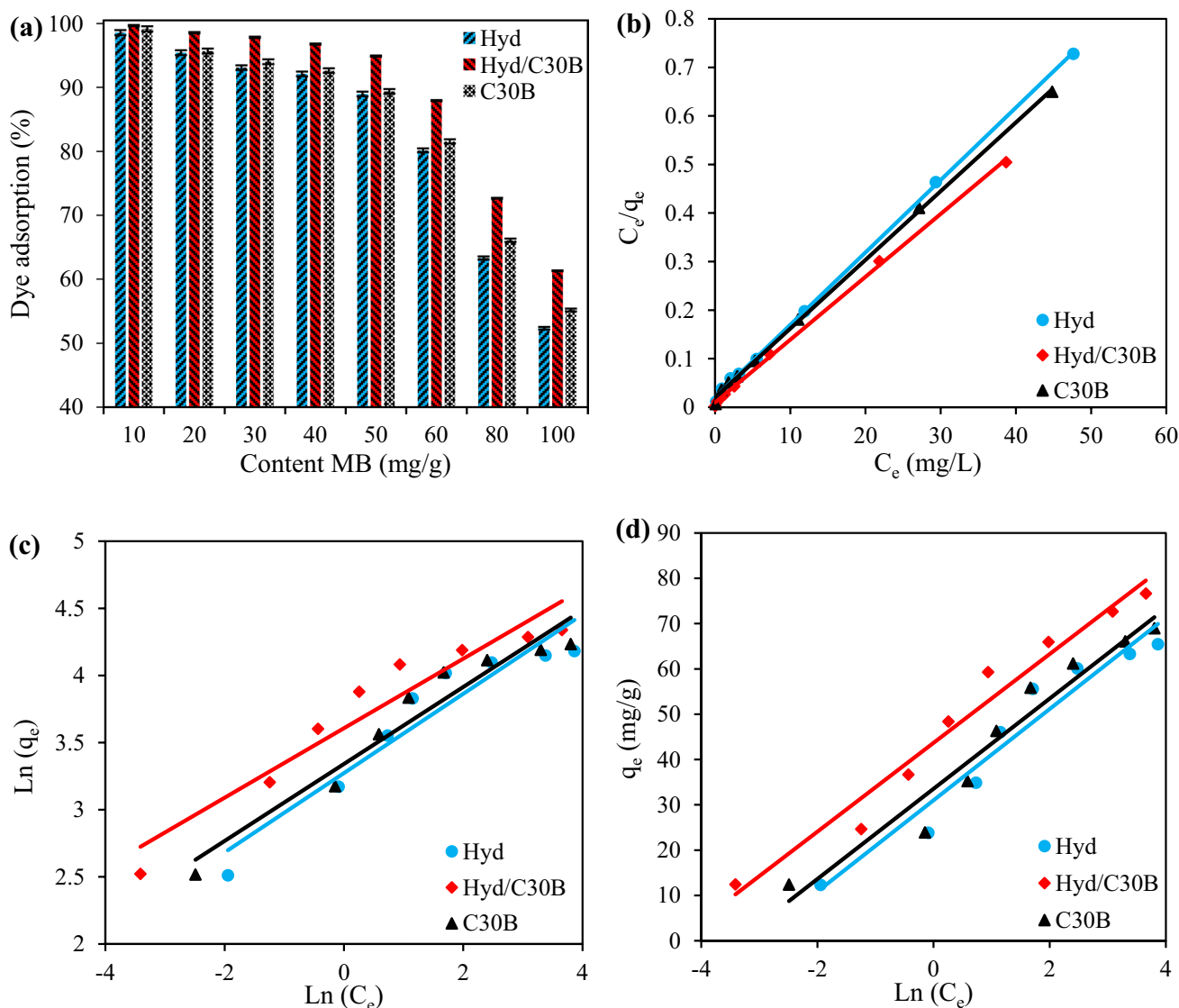


Fig. 7 (a) The effect of initial dye concentration on the adsorption efficiency (pH: 8, temperature: 45 °C, adsorbent dose: 0.8 g/L, time: 30 min, and mixing speed: 400 rpm), linear regression of isotherm

models (b) Langmuir, (c) Freundlich, and (d) Temkin for the MB adsorption using C30B, Hyd, and Hyd/C30B

implies adsorption intensity, K_T implies Temkin isotherm constant (L/g), R is the universal gas constant (kJ/mol.k), b implies the Temkin isotherm constant (kJ/mol) related to the energy parameter, and T is the absolute temperature (K).

To assess the adsorption process isotherm, the experimental values of C_e/q_e vs. C_e (Fig. 7b), $\ln(q_e)$ vs. $\ln(C_e)$ (Fig. 7c), and q_e vs. $\ln(C_e)$ (Fig. 7d) were plotted for Langmuir, Freundlich, and Temkin models, respectively. The isotherm factors are reported in Table 2. Due to the higher values of R^2 for the Langmuir isotherm than the other isotherm models, it is revealed that the isotherm data follow the Langmuir model. Therefore, according to this model, it can be said that MB molecules are homogeneously adsorbed on the monolayer surface of Hyd, Hyd/C30B, and C30B [50]. The maximum amount of monolayer adsorption capacity (q_m) was determined 67.114, 77.519, and 70.423 mg/g using Hyd, Hyd/C30B, and C30B, respectively. K_F parameter values for the MB dye adsorption process on Hyd, Hyd/C30B, and C30B are 26.385, 36.855, and 28.239 mg/g (L/mg)^{1/n}, respectively. Higher K_F values for Hyd/C30B indicate that Hyd/C30B has a greater tendency to adsorb MB molecules than Hyd and C30B. The values of $0 < R_L < 1$ and $n > 1$ indicate that the MB adsorption using the desired adsorbents is optimal and physical [51]. Also, the value of b_T reveals that the MB adsorption may include physical and chemical adsorption [52].

To evaluate the importance of the present study, the q_{max} values of monolayer adsorption in this work were compared with those reported in previous studies (Table 3). The comparison showed that the adsorbents have a good potential for MB removal from aqueous solutions compared to other adsorbents and they can be used as a vital option for eliminating MB from aqueous solutions.

Table 2 Isotherm parameters

Model	Parameter	Hyd	Hyd/C30B	C30B
Langmuir	$q_{e,exp}$ (mg/g) ^a	65.45	76.638	68.975
	$q_{e,max}$ (mg/g) _a	67.114	77.519	70.423
	K_L (L/mg)	0.723	1.344	0.696
	R_L	0.014–0.121	0.007–0.069	0.014–0.126
Freundlich	R^2	0.9994	0.9991	0.9991
	n	3.388	3.864	3.488
	K_F (mg/g (L/mg) ^{1/n})	26.385	36.855	28.239
Temkin	R^2	0.9052	0.9208	0.9361
	b_T (kJ/mol)	0.263	0.27	0.266
	K_T (L/g)	21.713	86.095	3.369
	R^2	0.9414	0.9675	0.949

^a $q_{e,exp}$ is q_e based on experimental and $q_{e,max}$ is the q_e based on calculation

Table 3 Comparison of the maximum MB adsorption capacity in different studies with the current study

Adsorbent	q_{max} (mg/g)	Ref
Zn-MOF	326	[53]
Carboxymethyl cellulose/carboxylated graphene oxide composite microbeads	183.23	[42]
Acid-activated kaolinite	58.8	[54]
chitosan-magadiite beads	40.01	[55]
Cal-Pal	57.47	[56]
P(AAm-co- Aconitic acid) Hydrogel	39.59	[57]
AC/CoFe2O4 composite	87.48	[29]
Hyd	67.114	present work
Hyd/C30B	77.519	present work
C30B	70.423	present work

Industrial wastewater treatment

To evaluate the wastewater treatment ability of the textile industry using Hyd, C30B, and Hyd/C30B, the sampled wastewater was first filtered to remove large solid particles. After the filtration process, the pH value of the prepared wastewater was adjusted to the optimal value, a certain amount of adsorbent was added to it, and then stirred for 60 min. After that, the ADMI parameter value was determined, which showed that by using Hyd, C30B, and Hyd/C30B, it was reduced from 942 to 247 (73.37%), 231 (75.47%), and 214 (77.28%), respectively. In addition, the amount of usual parameters in wastewater like COD, BOD₅, and TOC was significantly reduced by the studied adsorbents (see Table 4). Therefore, the results showed that the mentioned adsorbents can remove dyes from industrial wastewater and be used as vital adsorbents in industrial wastewater treatment.

Table 4 Characteristics of the textile industry

Characteristic	Fresh	Treated by		
		Hyd	C30B	Hyd/C30B
pH ¹	7.41	7.46	7.51	7.90
ADMI ²	942	247	231	214
COD (mg/L)	1,382	1309	1299	1271
BOD ₅ (mg/L)	637	614	608	582
TOC (mg/L)	406	389	384	380

¹Origin pH was 7.41, but it was regulated to 8

²ADMI: American Dye Manufactures Institute

Conclusions

Hyd and Hyd/C30B nanocomposite hydrogels were prepared using the free radical polymerization method and used in the MB adsorption. The effect of monomers, the amount of natural polymer CMC, and the value of C30B nanoclay on the swelling and adsorption performance of the samples were investigated. The presence of C30B in the nanocomposite hydrogel improved its BET area and MB sorption properties. Based on the operational parameters, the MB adsorption performance depended on swelling, factor groups, pores, and surface area. The swelling value of hydrogel systems was altered with changing the temperature and pH of the solution. The pseudo-second order kinetic and Langmuir isotherm models had a better ability to describe acquired data. The adsorbents had a good ability in treating industrial wastewater and can be utilized as a promising adsorbent in dye removal.

Supplementary Information The online version contains supplementary material available at <https://doi.org/10.1007/s10924-022-02623-x>.

Acknowledgements We would like to thank Ms. Batoul Azizi, the SEM operator in the Central Laboratory of Tabriz University, for doing SEM and Map-EDX analyzes.

Authors Contribution HK: Formal analysis, Methodology, Writing-original draft. SJP: Supervision, Conceptualization. RF: Conceptualization, Methodology. RM: Conceptualization, Methodology. BR: Writing- review& editing, Methodology, Supervision.

Funding This research did not receive any specific grant from funding agencies in the public, commercial, or not-for-profit sectors.

Data Availability The datasets used in this study are available from the corresponding author on reasonable request.

Declarations

Conflict of Interest The authors declare that they have no conflict of interest.

Consent to Publish All authors declare they have given consent to publish this article.

References

- Foroutan R, Mohammadi R, Ahmadi A, Bikhbar G, Babaei F, Ramavandi B (2022) Impact of ZnO and Fe₃O₄ magnetic nanoscale on the methyl violet 2B removal efficiency of the activated carbon oak wood. *Chemosphere* 286:131632
- Tang Y, Wang Q, Zhou B, Ma D, Ma Z, Zhu L (2015) Synthesis of sodium alginate graft poly (acrylic acid-co-acrylamide)/kaolin composite hydrogel and the study on its sorption of rhodamine B. *Polym Polym Compos* 23(7):467–474
- X.F. Sun, Z. Gan, Z. Jing, H. Wang, D. Wang, Y. Jin, Adsorption of methylene blue on hemicellulose-based stimuli-responsive porous hydrogel, *Journal of Applied Polymer Science* 132(10) (2015).
- Foroutan R, Peighambaroust SJ, Peighambaroust SH, Pateiro M, Lorenzo JM (2021) Adsorption of crystal violet dye using activated carbon of lemon wood and activated carbon/Fe₃O₄ magnetic nanocomposite from aqueous solutions: a kinetic, equilibrium and thermodynamic study. *Molecules* 26(8):2241
- Pashaei-Fakhri S, Peighambaroust SJ, Foroutan R, Arsalani N, Ramavandi B (2021) Crystal violet dye sorption over acrylamide/graphene oxide bonded sodium alginate nanocomposite hydrogel. *Chemosphere* 270:129419
- Rashidzadeh A, Olad A (2014) Slow-released NPK fertilizer encapsulated by NaAlg-g-poly (AA-co-AAm)/MMT superabsorbent nanocomposite. *Carbohydr Polym* 114:269–278
- Said M, Atassi Y, Tally M, Khatib H (2018) Environmentally friendly chitosan-g-poly (acrylic acid-co-acrylamide)/ground basalt superabsorbent composite for agricultural applications. *J Polym Environ* 26(9):3937–3948
- H. Mittal, A. Maity, S. Sinha Ray, The adsorption of Pb²⁺ and Cu²⁺ onto gum ghatti-grafted poly (acrylamide-co-acrylonitrile) biodegradable hydrogel: isotherms and kinetic models, *The Journal of Physical Chemistry B* 119(5) (2015) 2026–2039.
- M. Constantin, S.-M. Bucatariu, F. Doroftei, G. Fundueanu (2017) Smart composite materials based on chitosan microspheres embedded in thermosensitive hydrogel for controlled delivery of drugs. *Carbohydr Polym* 157:493–502
- Fosso-Kankeu E, Mittal H, Mishra SB, Mishra AK (2015) Gum ghatti and acrylic acid based biodegradable hydrogels for the effective adsorption of cationic dyes. *J Ind Eng Chem* 22:171–178
- Mittal H, Jindal R, Kaith B, Maity A, Ray S (2015) Flocculation and adsorption properties of biodegradable gum-ghatti-grafted poly (acrylamide-co-methacrylic acid) hydrogels. *Carbohydr Polym* 115:617–628
- Esposito A, Raccurt O, Charneau J-Y, Duchet-Rumeau J (2010) Functionalization of Cloisite 30B with fluorescent dyes. *Appl Clay Sci* 50(4):525–532
- Zhang J, Wang Q, Wang A (2007) Synthesis and characterization of chitosan-g-poly (acrylic acid)/attapulgit superabsorbent composites. *Carbohydr Polym* 68(2):367–374
- Anirudhan T, Rijith S (2012) Synthesis and characterization of carboxyl terminated poly (methacrylic acid) grafted chitosan/bentonite composite and its application for the recovery of uranium (VI) from aqueous media. *J Environ Radioact* 106:8–19
- X.-F. Sun, Y. Hao, Y. Cao, Q. Zeng, Superadsorbent hydrogel based on lignin and montmorillonite for Cu(II) ions removal from aqueous solution, *International Journal of Biological Macromolecules* 127 (2019) 511–519. <https://doi.org/10.1016/j.ijbiomac.2019.01.058>.
- Reddy BN, Rauta PR, Venkatalakshmi V, Sreenivasa S (2018) Synthesis and characterization of cloisite-30B clay dispersed poly (acryl amide/sodium alginate)/AgNp hydrogel composites for the study of BSA protein drug delivery and antibacterial activity. *Materials Research Express* 5(2):025403
- H. Dai, Y. Zhang, L. Ma, H. Zhang, H. Huang, Synthesis and response of pineapple peel carboxymethyl cellulose-g-poly (acrylic acid-co-acrylamide)/graphene oxide hydrogels, *Carbohydrate Polymers* 215 (2019) 366–376. <https://doi.org/10.1016/j.carbpol.2019.03.090>.
- Bagheri N, Lakouraj MM, Hasantabar V, Mohseni M (2021) Biodegradable macro-porous CMC-polyaniline hydrogel: synthesis, characterization and study of microbial elimination and sorption capacity of dyes from waste water. *J Hazard Mater* 403:123631
- Wang H, Li Z, Yahyaoui S, Hanafy H, Seliem MK, Bonilla-Petriciolet A, Dotto GL, Sellaoui L, Li Q (2021) Effective adsorption of dyes on an activated carbon prepared from carboxymethyl

- cellulose: Experiments, characterization and advanced modelling. *Chem Eng J* 417:128116
20. Gad YH, Ali HE, Hegazy A (2021) Synergistic effect of titanium dioxide (TiO₂) and ionizing radiation on thermal and mechanical properties of carboxymethyl cellulose (CMC) for potential application in removal of basic dye from wastewater. *J Polym Environ* 29(12):3887–3899
 21. M.C.I. Mohd Amin, N. Ahmad, M. Pandey, C. Jue Xin, Stimuli-responsive bacterial cellulose-g-poly (acrylic acid-co-acrylamide) hydrogels for oral controlled release drug delivery, *Drug development and industrial pharmacy* 40(10) (2014) 1340–1349.
 22. Ariaeenejad S, Hosseini E, Motamedi E, Moosavi-Movahedi AA, Salekdeh GH (2019) Application of carboxymethyl cellulose-g-poly (acrylic acid-co-acrylamide) hydrogel sponges for improvement of efficiency, reusability and thermal stability of a recombinant xylanase. *Chem Eng J* 375:122022
 23. Ramadan AR, Esawi AM, Gawad AA (2010) Effect of ball milling on the structure of Na⁺-montmorillonite and organo-montmorillonite (Cloisite 30B). *Appl Clay Sci* 47(3–4):196–202
 24. Esmaeili H, Foroutan R (2019) Adsorptive Behavior of Methylene Blue onto Sawdust of Sour Lemon, Date Palm, and Eucalyptus as Agricultural Wastes. *J Dispersion Sci Technol* 40(7):990–999. <https://doi.org/10.1080/01932691.2018.1489828>
 25. Bao Y, Ma J, Li N (2011) Synthesis and swelling behaviors of sodium carboxymethyl cellulose-g-poly (AA-co-AM-co-AMPS)/MMT superabsorbent hydrogel. *Carbohydr Polym* 84(1):76–82
 26. S. El-Sayed, K. Mahmoud, A. Fatah, A. Hassen, DSC, TGA and dielectric properties of carboxymethyl cellulose/polyvinyl alcohol blends, *Physica B: Condensed Matter* 406(21) (2011) 4068–4076.
 27. Yu J, Yang G, Li Y, Yang W, Gao J, Lu Q (2014) Synthesis, Characterization, and swelling behaviors of acrylic acid/carboxymethyl cellulose superabsorbent hydrogel by glow-discharge electrolysis plasma. *Polym Eng Sci* 54(10):2310–2320
 28. Ma Y-Z, Zheng D-F, Mo Z-Y, Dong R-J, Qiu X-Q (2018) Magnetic lignin-based carbon nanoparticles and the adsorption for removal of methyl orange. *Colloids Surf, A* 559:226–234
 29. Foroutan R, Mohammadi R, Ramavandi B (2019) Elimination performance of methylene blue, methyl violet, and Nile blue from aqueous media using AC/CoFe₂O₄ as a recyclable magnetic composite. *Environ Sci Pollut Res* 26(19):19523–19539
 30. Makhado E, Pandey S, Modibane KD, Kang M, Hato MJ (2020) Sequestration of methylene blue dye using sodium alginate poly (acrylic acid)@ ZnO hydrogel nanocomposite: kinetic, isotherm, and thermodynamic investigations. *Int J Biol Macromol* 162:60–73
 31. Wu F, Zhang Y, Liu L, Yao J (2012) Synthesis and characterization of a novel cellulose-g-poly (acrylic acid-co-acrylamide) superabsorbent composite based on flax yarn waste. *Carbohydr Polym* 87(4):2519–2525
 32. He G, Ke W, Chen X, Kong Y, Zheng H, Yin Y, Cai W (2017) Preparation and properties of quaternary ammonium chitosan-g-poly (acrylic acid-co-acrylamide) superabsorbent hydrogels. *React Funct Polym* 111:14–21
 33. Olad A, Zebhi H, Salari D, Mirmohseni A, Reyhanitabar A (2018) A promising porous polymer-nanoclay hydrogel nanocomposite as water reservoir material: synthesis and kinetic study. *J Porous Mater* 25(3):665–675
 34. Mohammadinezhad A, Marandi GB, Farsadrooh M, Javadian H (2018) Synthesis of poly (acrylamide-co-itaconic acid)/MWCNTs superabsorbent hydrogel nanocomposite by ultrasound-assisted technique: swelling behavior and Pb (II) adsorption capacity. *Ultrason Sonochem* 49:1–12
 35. Oveisi M, Asli MA, Mahmoodi NM (2018) MIL-Ti metal-organic frameworks (MOFs) nanomaterials as superior adsorbents: Synthesis and ultrasound-aided dye adsorption from multicomponent wastewater systems. *J Hazard Mater* 347:123–140
 36. Jana S, Ray J, Mondal B, Pradhan S, Tripathy T (2018) pH responsive adsorption/desorption studies of organic dyes from their aqueous solutions by katira gum-cl-poly (acrylic acid-co-N-vinyl imidazole) hydrogel. *Colloids Surf, A* 553:472–486
 37. Foroutan R, Peighambari SJ, Hosseini SS, Akbari A, Ramavandi B (2021) Hydroxyapatite biomaterial production from chicken (femur and beak) and fishbone waste through a chemical less method for Cd²⁺ removal from shipbuilding wastewater. *J Hazard Mater* 413:125428
 38. Foroutan R, Mohammadi R, MousaKhanloo F, Sahebi S, Ramavandi B, Kumar PS, Vardhan KH (2020) Performance of montmorillonite/graphene oxide/CoFe₂O₄ as a magnetic and recyclable nanocomposite for cleaning methyl violet dye-laden wastewater. *Adv Powder Technol* 31(9):3993–4004
 39. Fabryanty R, Valencia C, Soetaredjo FE, Putro JN, Santoso SP, Kurniawan A, Ju Y-H, Ismadji S (2017) Removal of crystal violet dye by adsorption using bentonite–alginate composite. *J Environ Chem Eng* 5(6):5677–5687
 40. Shirsath S, Hage A, Zhou M, Sonawane S, Ashokkumar M (2011) Ultrasound assisted preparation of nanoclay Bentonite-FeCo nanocomposite hybrid hydrogel: a potential responsive sorbent for removal of organic pollutant from water. *Desalination* 281:429–437
 41. Hosseinzadeh H, Ramin S (2018) Fabrication of starch-graft-poly (acrylamide)/graphene oxide/hydroxyapatite nanocomposite hydrogel adsorbent for removal of malachite green dye from aqueous solution. *Int J Biol Macromol* 106:101–115
 42. Eltaweil AS, Elgarhy GS, El-Subruiti GM, Omer AM (2020) Carboxymethyl cellulose/carboxylated graphene oxide composite microbeads for efficient adsorption of cationic methylene blue dye. *Int J Biol Macromol* 154:307–318
 43. Chakraborty R, Verma R, Asthana A, Vidya SS, Singh AK (2021) Adsorption of hazardous chromium (VI) ions from aqueous solutions using modified sawdust: kinetics, isotherm and thermodynamic modelling. *Int J Environ Anal Chem* 101(7):911–928
 44. C.P. Bergmann, F.M. Machado, Carbon nanomaterials as adsorbents for environmental and biological applications, Springer 2015.
 45. An C, Yang S, Huang G, Zhao S, Zhang P, Yao Y (2016) Removal of sulfonated humic acid from aqueous phase by modified coal fly ash waste: equilibrium and kinetic adsorption studies. *Fuel* 165:264–271
 46. Foroutan R, Peighambari SJ, Latifi P, Ahmadi A, Alizadeh M, Ramavandi B (2021) Carbon nanotubes/β-cyclodextrin/MnFe₂O₄ as a magnetic nanocomposite powder for tetracycline antibiotic decontamination from different aqueous environments. *J Environ Chem Eng* 9(6):106344
 47. Foroutan R, Peighambari SJ, Hemmati S, Khatooni H, Ramavandi B (2021) Preparation of clinoptilolite/starch/CoFe₂O₄ magnetic nanocomposite powder and its elimination properties for cationic dyes from water and wastewater. *Int J Biol Macromol* 189:432–442
 48. Foo KY, Hameed BH (2010) Insights into the modeling of adsorption isotherm systems. *Chem Eng J* 156(1):2–10
 49. Priastomo Y, Setiawan HR, Kurniawan YS, Ohto K (2020) Simultaneous removal of lead (II), chromium (III), and copper (II) heavy metal ions through an adsorption process using C-phenylcalix [4] pyrogallolarene material. *J Environ Chem Eng* 8(4):103971
 50. El Haouti R, Ouachtak H, El Guerdaoui A, Amedlous A, Amaterz E, Haounati R, Addi AA, Akbal F, El Alem N, Taha ML (2019) Cationic dyes adsorption by Na-Montmorillonite Nano Clay: Experimental study combined with a theoretical investigation using DFT-based descriptors and molecular dynamics simulations. *J Mol Liq* 290:111139
 51. Yusuff AS, Owolabi JO, Igbomezie CO (2021) Optimization of process parameters for adsorption of heavy metals from aqueous

- solutions by alumina-onion skin composite. *Chem Eng Commun* 208(1):14–28
52. Hu X-J, Wang J-S, Liu Y-G, Li X, Zeng G-M, Bao Z-L, Zeng X-X, Chen A-W, Long F (2011) Adsorption of chromium (VI) by ethylenediamine-modified cross-linked magnetic chitosan resin: isotherms, kinetics and thermodynamics. *J Hazard Mater* 185(1):306–314
53. Zhang J, Li F, Sun Q (2018) Rapid and selective adsorption of cationic dyes by a unique metal-organic framework with decorated pore surface. *Appl Surf Sci* 440:1219–1226
54. Sarma GK, SenGupta S, Bhattacharyya KG (2011) Methylene blue adsorption on natural and modified clays. *Sep Sci Technol* 46(10):1602–1614
55. Mokhtar A, Abdelkrim S, Djelad A, Sardi A, Boukoussa B, Sassi M, Bengueddach A (2020) Adsorption behavior of cationic and anionic dyes on magadiite-chitosan composite beads. *Carbohydr Polym* 229:115399
56. Youcef LD, Belaroui LS, López-Galindo A (2019) Adsorption of a cationic methylene blue dye on an Algerian palygorskite. *Appl Clay Sci* 179:105145
57. Işikver Y (2017) Removal of some cationic dyes from aqueous solution by acrylamide-or 2-hydroxyethyl methacrylate-based copolymeric hydrogels. *Fibers and Polymers* 18(11):2070–2078

Publisher's Note Springer Nature remains neutral with regard to jurisdictional claims in published maps and institutional affiliations.

Springer Nature or its licensor (e.g. a society or other partner) holds exclusive rights to this article under a publishing agreement with the author(s) or other rightsholder(s); author self-archiving of the accepted manuscript version of this article is solely governed by the terms of such publishing agreement and applicable law.